

Bringing GPS into harsh environments for fully automated deformation monitoring

Jason Bond · Adam Chrzanowski · Don Kim

Received: 16 October 2006 / Accepted: 12 February 2007 / Published online: 13 March 2007
© Springer-Verlag 2007

Abstract Engineering projects that require deformation monitoring frequently utilize geodetic sensors to measure displacements of target points located in the deformation zone. In situations where control stations and targets are separated by a kilometer or more, GPS can offer higher precision position updates at more frequent intervals than can normally be achieved using total station technology. For large-scale deformation projects requiring the highest precision, it is therefore advisable to use a combination of the two sensors. In response to the need for high precision, continuous GPS position updates in harsh deformation monitoring environments, a software has been developed that employs triple-differenced carrier-phase measurements in a delayed-state Kalman filter. Two data sets were analyzed to test the capabilities of the software. In the first test, a GPS antenna was displaced using a translation stage to mimic slow deformation. In the second test, data collected at a large open pit mine were processed. It was shown that the delayed-state Kalman filter developed could detect millimeter-level displacements of a GPS antenna. The actual precision attained depends upon the amount of process noise infused at each epoch to accommodate the antenna displacements. Higher process noise values result in quicker detection times, but at the same time increase the noise in the solutions. A slow, 25 mm displacement was detected within 30 min of the full displacement with sigma values in

E , N and U of ± 10 mm or better. The same displacement could also be detected in less than 5 h with sigma values in E , N and U of ± 5 mm or better. The software works best for detecting long period deformations (e.g., 20 mm per day or less) for which sigma values of 1–2 mm are attained in all three solution components. It was also shown that the triple-differenced carrier-phase observation can be used to significantly reduce the effects of residual tropospheric delay that would normally plague double-differenced observations in harsh GPS environments.

Keywords GPS · Deformation monitoring · Triple-differenced · Kalman filter

Introduction

Disasters resulting from the collapse of steep embankments or structures (e.g., avalanches, mudslides, dam failure, collapsing of roofs) do not occur without warning. Strategic monitoring in a hazardous area can create an awareness of any impending danger, resulting in quicker emergency response times and disaster prevention. The Canadian Centre for Geodetic Engineering's fully automated deformation monitoring system, ALERT, has been implemented worldwide for such purposes (Wilkins et al. 2003).

The ALERT system uses robotic total station (RTS) instruments with automatic target recognition as its primary sensors. RTS instruments are presently the most economical method of monitoring displacements when hundreds of target points must be observed in the deformation zone. This approach, however, has its limitations.

When distances between total stations and targets increase, the effects of atmospheric refraction biases and pointing errors become dominant (Chrzanowski and Wil-

J. Bond (✉) · A. Chrzanowski · D. Kim
University of New Brunswick, P.O. Box 4400,
Fredericton, NB, Canada E3B 5A3
e-mail: jason.bond@unb.ca

A. Chrzanowski
e-mail: adamc@unb.ca

D. Kim
e-mail: kim@unb.ca

kins 2006). If sight lengths are too long, these error sources will result in accuracy requirements not being met. In order to optimize the accuracy, it is not uncommon to place the RTSs within the deformation zone, so that they are as close as possible to the targets (Bond et al. 2005). In such cases, the use of GPS to monitor the stability of the RTSs is recommended. GPS allows the RTSs to be connected to stable reference points while avoiding these concerns. Implementing GPS for this purpose, however, poses its own challenges.

Discussed is a response to the need for the development of a robust GPS software to provide high precision, fully automated position updates for the purpose of deformation monitoring. Requirements for the system are listed and the challenges associated with meeting them are given. The test results are presented demonstrating the advantages of this approach over traditional batch processing methods.

System requirements

To meet the needs of deformation monitoring applications, the developed system should have the following characteristics:

- Fully automated: position updates must be provided without human intervention. Intelligence must be instilled in the system so that it can handle contingencies (e.g., power outages, poor data and sudden displacements).
- On-time updates: the user must be made aware of unexpected structural behavior as quickly as possible, so that notice can be given of impending danger. The system must be capable of providing deformation information at regular intervals as dictated by project specifications.
- Robust: false alarms cannot be tolerated. Quality assurance/quality control measures must be reliable so that there is confidence in the system.
- High precision: displacements encountered in deformation monitoring are frequently at the sub-centimeter level. Since the practical resolution of an undifferenced GPS carrier-phase measurement is approximately 2 mm (1% of the L1 carrier wavelength of 0.190 m), monitoring millimeter-level displacements in near real-time pushes the limits of the system. If millimeter-level precision is to be achieved, meticulous effort and care must be devoted to handling all error sources.

Challenges in meeting requirements

Achieving reliable, millimeter-level precision in ‘real-time’ using GPS is challenging in favorable monitoring

conditions. Attempting to do the same in harsh environments is even more difficult. Presented are some of the challenges faced in designing a system that meets deformation monitoring needs, as were discussed in Kim et al. (2003).

Satellite visibility

In deformation monitoring environments where there are obstructions hindering satellite visibility (e.g., dams, open pit mines, buildings), dilution of precision values rise due to the degradation in satellite geometry. The system must be able to cope with periods of the day during which there are too few satellites visible to provide a high enough quality solution to meet project requirements.

Residual tropospheric delay

In deformation monitoring environments where there are significant changes in elevation (e.g., open pit mines, volcanoes), residual tropospheric delay can cause significant positioning biases, especially in height. The differential troposphere causes a 3–5 mm relative height error for every millimeter difference in zenith delay between stations (Beutler et al. 1988). Residual tropospheric delay must be accounted for if the desired precision is to be achieved.

Multipath

In deformation monitoring environments where multipath sources are abundant (e.g., building structures, vehicles) multipath can contaminate the position solutions. Practically, every observation site is affected to some degree by multipath. Multipath biases can reach up to $\lambda/4 \approx 4.8$ cm for the original L1 carrier-phase measurement (Leick 1994).

Providing on-time information

Deformation monitoring poses a unique GPS scenario; the points of interest are neither quite static nor kinematic because there is motion, but it is usually very small. In providing GPS position updates, it cannot be assumed that the antenna’s position at an epoch agrees with that of a prior epoch. One way to handle this is to model the motion as static and to add process noise.

PPMS software description

With regard to the above-mentioned requirements and concerns, software is being developed to provide high precision position updates in the harshest deformation moni-

toring environments. Some of the details of Precise Position Monitoring System (PPMS) are presented. Future work will be devoted to making the software fully automated.

Choice of observable

The double-differenced (DD: differencing between receivers followed by differencing between satellites or vice versa), ambiguity-fixed carrier-phase observation is the most commonly used GPS measurement for high precision applications. This observation type allows for quick convergence on a solution once the ambiguity term has been resolved. The ambiguity term is always present, however, which leaves the possibility of false alarms caused by poorly handled cycle slips.

Remondi (1984) demonstrated the potential for using the triple-differenced (TD: differencing consecutive DD observations) observable as an alternative method of obtaining high precision. Despite introducing another level of differencing, which increases the observation noise, the TD approach offers several advantages over the DD, ambiguity-fixed observable making it an attractive alternative. After removing the error terms for receiver clocks and satellite clocks (which should be eliminated through DD processing when observation simultaneity criteria are met), the TD, carrier-phase observable between times t_1 and t_2 can be written as:

$$\delta \Delta \nabla_{AB}^{ij} \varphi(t_{12}) = [\Delta \nabla_{AB}^{ij}(\varphi + N + M - \frac{f}{c}I + \frac{f}{c}T + e_{\varphi}) + \varepsilon_{\text{trop}}]_{t_2} - [\Delta \nabla_{AB}^{ij}(\varphi + N + M - \frac{f}{c}I + \frac{f}{c}T + e_{\varphi}) + \varepsilon_{\text{trop}}]_{t_1} \tag{1}$$

where

- ∇_{ij} single-difference (SD) operator between satellites i and j
- Δ SD operator between receivers A and B
- Δ_{AB} SD operator between times t_1 and t_2
- φ carrier-phase observable (cycles)
- N ambiguity (cycles)
- M multipath (cycles)
- I ionospheric delay of the L1 carrier phase (m)
- T tropospheric delay (m)
- f carrier wave frequency (Hz)
- c speed of light in a vacuum (m/s)
- $\varepsilon_{\text{trop}}$ residual tropospheric delay bias (present over large height differences) (cycles)
- e_{φ} random carrier-phase measurement noise.

The TD approach can be considered to be an extension of the observation difference, least squares approach used

for processing deformation monitoring data (Wilkins et al. 2003). The attractiveness of the TD observation is that it is a time difference of DD observations and consequently any biases common to both observations will be highly correlated and therefore significantly reduced. This strategy has some important benefits:

- The user no longer needs to solve the ambiguity term, which allows the system to be more robust.
- For observation intervals less than a few seconds, the correlation between atmospheric parameters between times t_1 and t_2 will be large and therefore biases originating from them will be significantly reduced. This is useful for dealing with residual tropospheric delay biases over large height differences.
- For observation intervals less than a few seconds, the correlation in the low frequency component of multipath terms at times t_1 and t_2 will be large and therefore biases originating from them will be significantly reduced. The high frequency component still remains.

Equation (1) can now be rewritten as:

$$\delta \Delta \nabla_{AB}^{ij} \varphi(t_{12}) = [\Delta \nabla_{AB}^{ij}(\varphi + M)]_{t_2} - [\Delta \nabla_{AB}^{ij}(\varphi + M)]_{t_1} + e_{\delta \Delta \nabla \varphi} \tag{2}$$

where

$e_{\delta \Delta \nabla \varphi}$ random noise error of a TD carrier-phase observation.

From Eq. (2) it can be seen that through the differencing process, most major error sources can be significantly reduced so that the main remaining sources of error are the random noise error inherent in the TD observable and the high frequency component of multipath. The major disadvantage of the TD approach is that it requires a longer convergence time than for DD processing.

Processing engine

Batch processing involves the estimation of a static set of unknown parameters. Each set of observations is used to provide a better estimate of the same quantities. Deformation monitoring requires an awareness of the current state of the deformable body rather than an overall average of all previous states. Kalman filtering or modified sequential least squares data processing techniques are preferable since they are able to provide a snapshot image of the current state of the unknown parameters (in this case, the same results can be achieved using Kalman filtering and sequential least squares by introducing process noise into the sequential least squares solution, since there are no dynamics in the transition matrix).

The TD observation is an integrated velocity over some time interval, Δt . Model and measurement situations of this type fit the delayed-state form (Brown and Hwang 1997):

$$x_{k+1} = \phi_k x_k + w_k; \quad E[w_k w_k^T] = Q_k \quad (3)$$

$$z_k = H_k x_k + J_k x_{k-1} + v_k; \quad E[v_k v_k^T] = R_k \quad (4)$$

where

x_k process state vector at time t_k (x, y, z coordinates of the station)

ϕ_k transition matrix at time t_k (identity matrix—no dynamics)

w_k model error at time t_k (white sequence)

z_k TD observations at time t_k

H_k DD design matrix at time t_k

J_k negated DD design matrix at time t_{k-1} ¹

v_k observation error at time t_k (white sequence)

The delayed-state recursive equations are presented in Table 1.

The delayed-state Kalman filter implemented is built upon that introduced by Remondi and Brown (2000). The major difference in the two filters lies in their approaches to handling observation and process noise. Remondi and Brown (2000) estimate the noise as Gauss-Markov parameters. The approach used in PPMS is to estimate each satellite's carrier-phase observation noise to populate the R_k matrix. This is accomplished by using the time-differenced, geometry-free (GF: differencing between L1 and L2 in the distance unit) SD (between receivers) of each satellite as a measure of the satellite's current noise state. Because the GF combination is used, antenna dynamics are eliminated from the noise estimation process.

The approach employed corresponds to high-pass filtering, as most low-frequency errors in the carrier-phase measurements are significantly reduced. Satellite clock errors are eliminated through the between receivers SD. Tropospheric delay biases are eliminated through the GF combination. Ionospheric delay biases are significantly reduced through the SD process. Between epochs time-differencing further reduces the effects of ionospheric delay and significantly reduces any low-frequency component multipath biases. The remaining measurement noise, thermal noise of the receiver and high frequency component

multipath biases are used as a measure of the satellite's current noise state. A moving average window is then used to improve the estimate based upon the past n measures of noise, where n is the window size.

The Q_k matrix is a diagonal matrix of Q values. The Q value is a noise parameter that is used to accommodate the expected velocity of the antenna. It dictates how quickly the filter responds to displacements by changing the weight placed on previous solutions and current observations. There is no single correct Q value. Rather, the Q value chosen is dependent upon the magnitude of the expected displacements, the length of time over which the displacement occurs, the sample rate of the observations and the delay in detection time that can be tolerated.

For example, if one anticipates a 0.005 m displacement in 10 s, the sample rate is 10 s and the displacement must be detected immediately, then a Q value of $(0.005 \text{ m})^2$ may be appropriate. If a 30 min delay in detection time can be tolerated, then a Q value of $(0.005 \text{ m})^2/1,800 \text{ s}/10 \text{ s} = (0.37 \text{ mm})^2$ may be used. Using a larger Q value increases the size of the minimum detectable bias (MDB). Consequently, there is a tradeoff between detection time and MDB. Alternatively, if the Q value is too small, the filter will not be able to track the displacements and will diverge.

From a theoretical standpoint, the performance of the filter may not be optimal. This is due to the fact that there are potentially non-white components in the observation noise matrices caused by small residual biases that may have not been eliminated through differencing. In practicality, the filter has demonstrated good results.

Cycle slip detection

Even though the TD observable eliminates common integer ambiguities, cycle slips still need to be identified and removed to prevent outliers from existing in the observations. The approach used here is based upon that of Kim and Langley (2002), which allows for instantaneous, real-time cycle-slip detection. The GF, TD observations are compared against a cycle slip threshold. Observations exceeding this threshold are discarded.

Outlier detection

PPMS currently utilizes an often used "rule of thumb" in detecting outliers that reject any observation with a residual exceeding three times the standard deviation of the observations (Rizos 1999). The software is currently being modified to allow for a more sophisticated outlier detection mechanism that compares the predicted and computed residuals of the Kalman filter (Teunissen 1998).

¹ The TD design matrix is the difference of the current and previous DD design matrices. The x, y, z coordinates of the station are treated as constant when populating these matrices. The computed TD observations depend upon the changes in satellite geometry from t_{k-1} to t_k . Over high sample rates these values will be small and so care must be taken to carry sufficient precision.

Table 1 Delayed-state equations (Brown and Hwang 1997)

Estimate update:	$x_k = x_k^- + K_k(z_k - \hat{z}_k^-)$
where	$\hat{z}_k^- = H_k \hat{x}_k^- + J_k \hat{x}_{k-1}$
Gain:	$K_k = [P_k^- H_k^T + \phi_{k-1} P_{k-1} J_k^T] L_k^{-1}$
where	$L_k = H_k P_k^- H_k^T + R_k + J_k P_{k-1} \phi_{k-1}^T H_k^T + H_k \phi_{k-1} P_{k-1} J_k^T + J_k P_{k-1} J_k^T$
Error covariance update:	$P_k = P_k^- - K_k L_k K_k^T$
Predictions:	$\hat{x}_{k+1}^- = \phi_k \hat{x}_k$ $P_{k+1}^- = \phi_k P_k \phi_k^T + Q_k$

Tests

Two data sets are presented to illustrate the performance of the software. The first data set was observed on the roof of Head Hall at the University of New Brunswick. A translation stage was used to introduce displacements to the rover antenna to determine the sensitivity of the filter. The second data set comes from a large open pit mine, representing a harsh GPS environment. NovAtel DL4 receivers with GPS-600 Pinwheel antennas were used in all tests.

Data were processed using PPMS implementing a 10° elevation cut-off angle and the UNB3 tropospheric model (Saastamoinen zenith delay with lookup tables) with Niell mapping functions (Collins and Langley 1999). The results were compared with DD, ambiguity-fixed solutions from commercial software using the same elevation cut-off angle and Saastamoinen tropospheric model with unknown mapping functions. The sample rate for both data sets was 10 s.

Translation stage test

Using a translation stage to mimic slow displacements caused by deformation, a short baseline (~20 m) was ob-



Fig. 1 Translation stage test

Table 2 Displacements introduced with translation stage

Elapsed time (h)	Displacement introduced (mm) (total)	Displacement time (s)
20:00:00	2 (2)	10
20:31:50	2 (4)	10
21:00:00	2 (6)	10
21:25:00	2 (8)	10
22:30:00	2 (10)	10
23:00:00	5 (15)	25
23:32:00	5 (20)	25
24:00:00	5 (25)	25

served to gain an appreciation for the sensitivity of the filter (see Fig. 1). Approximately, 20 h of data were collected before moving the antenna. Table 2 illustrates the sequence of displacements introduced using the translation stage. The data were processed using different *Q* values to illustrate the impact of this matrix on the solutions.

Translation stage results

In this test, displacements of magnitude 2 and 5 mm were introduced. The 2 mm displacements occur over a 10 s period and the 5 mm displacements occur over a 25 s period. The duration between displacements is approximately 30 min. In the first case, a *Q* value was chosen to accommodate 5 mm displacements every 30 min [$Q = (5 \text{ mm})^2/1,800 \text{ s}/10 \text{ s} = (0.4 \text{ mm})^2$]. The *E*, *N*, *U* displacements detected by PPMS are shown in Fig. 2. The solid lines crossing the *x*-axis indicate the beginning (green) of the movements of the translation stage and the end (red). Averaging the solutions over the last hour of the experiment results in detected displacements of 15 and 14 mm in the east and north components, respectively, for a total detected displacement of 21 mm. The full displacements are detected within 30 min of being introduced. After convergence, the average standard deviations in *E*, *N*, *U* components are ±10, 7 and 9 mm, respectively. Interestingly, the more dramatic changes in satellite geometry in the north and up components allow for better displacement detection in these components than in the east component.

In the second case, a *Q* value was chosen to accommodate 3 mm displacements every 30 min [$Q = (0.2 \text{ mm})^2$]. The *E*, *N*, *U* displacements detected by PPMS are shown in Fig. 3. Averaging the solutions over the last hour of the experiment results in detected displacements of 17 and 15 mm in the east and north components, respectively, for a total detected displacement of 23 mm. There is about a 1 h delay in detecting the full displacement due to the actual velocity of the antenna exceeding the predicted velocity, as represented by the *Q*

Fig. 2 Detected translation stage displacements for $Q = (0.4 \text{ mm})^2$

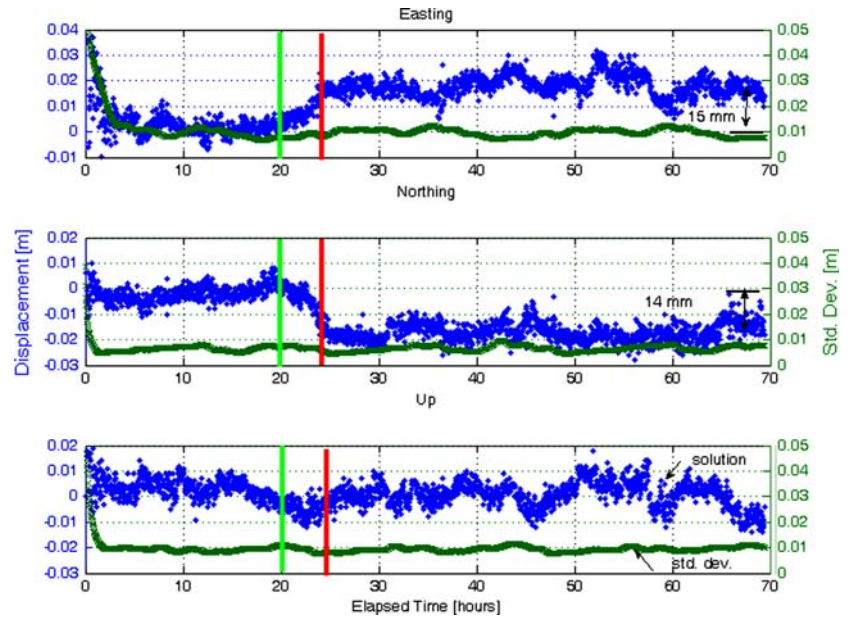
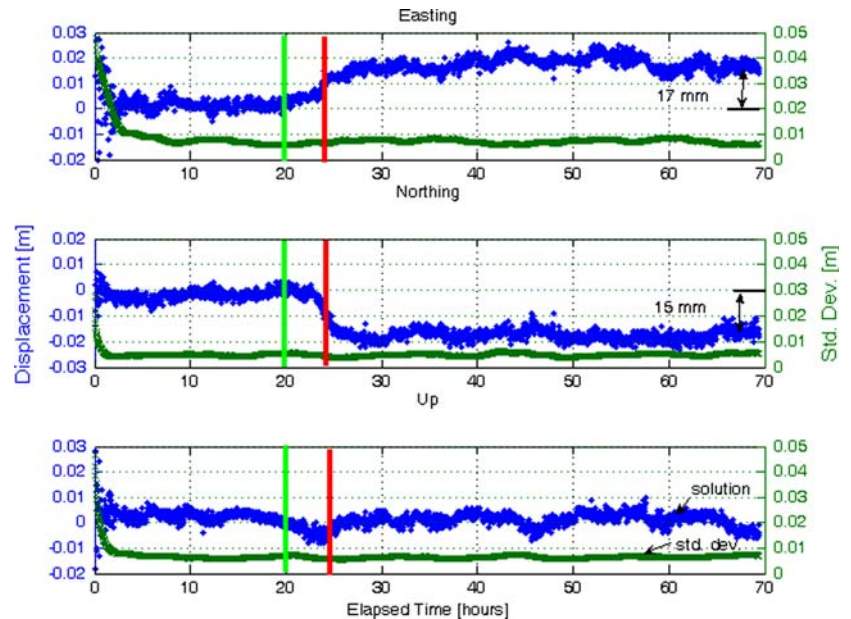


Fig. 3 Detected translation stage displacements for $Q = (0.2 \text{ mm})^2$



value. After convergence, the average standard deviations in E , N , U components are ± 7 , 5 and 6 mm, respectively.

In the third case, a Q value was chosen to accommodate 1.5 mm displacements every 30 min [$Q = (0.1 \text{ mm})^2$]. The E , N , U displacements detected by PPMS are shown in Fig. 4. Averaging the solutions over the last hour of the experiment results in detected displacements of 17 and 17 mm in the east and north components, respectively, for a total detected displacement of 24 mm. There is about a 4.5 h delay in detecting the full displacement due to the actual velocity of the antenna exceeding the predicted velocity, as represented by the Q value. After convergence,

the average standard deviations in E , N , U components are ± 5 , 3 and 4 mm, respectively.

Finally, a fourth case was investigated to gain an appreciation for the achievable precision of the filter when slower displacements are expected. In this scenario, a Q value was chosen to accommodate 0.75 mm displacements every 30 min [$Q = (0.05 \text{ mm})^2$]. Averaging the solutions over the last hour of the experiment results in detected displacements of 18 and 17 mm in the east and north components, respectively, for a total detected displacement of 25 mm. There is about a 15 h delay in detecting the full displacement due to the actual velocity of the antenna

Fig. 4 Detected translation stage displacements for $Q = (0.1 \text{ mm})^2$

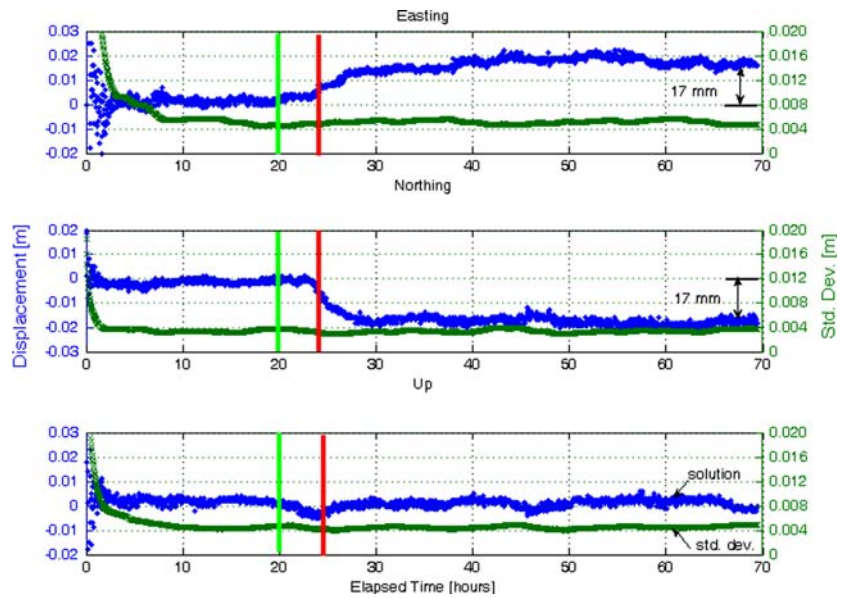


Table 3 Displacement detection summary

Q value	Approximate displacement rate accommodated (mm/30 min)	Delay in detecting full displacement (h)	σ_E (\pm mm)	σ_N (\pm mm)	σ_U (\pm mm)
$(0.4 \text{ mm})^2$	5	0.5	10	7	9
$(0.2 \text{ mm})^2$	3	1	7	5	6
$(0.1 \text{ mm})^2$	1.5	4.5	5	3	4
$(0.05 \text{ mm})^2$	0.75	15	3	3	3

exceeding the predicted velocity, as represented by the Q value. After convergence, the average standard deviations in E, N, U components are $\pm 3, 3$ and 3 mm, respectively.

Larger Q values allow the filter to put more emphasis on the measurements and therefore respond more quickly to the displacements. At the same time, the noise level increases in the solutions. Table 3 summarizes the results of the four scenarios investigated. Column 3—“Delay in detecting full displacement”—represents the length of time after the series of small displacements were introduced that was required to detect the full 25 mm displacement. In all cases investigated, the delay in detecting the full displacement would be approximately 30 min if the actual displacements introduced occurred at the rate prescribed by the Q value.

The filter’s delay in detecting displacements is dependent upon the process noise value, Q , the change in satellite geometry and the accuracy of the noise model of the observations (used to populate R). If slow deformations are anticipated (e.g., up to 20 mm per day), then a very small Q value can be used (e.g., 0.001) and sigma values of 2 mm or better can be attained in all three solution components. Further research is required to determine a method of implementing an adaptive Q value that would allow for quicker displacement detection.

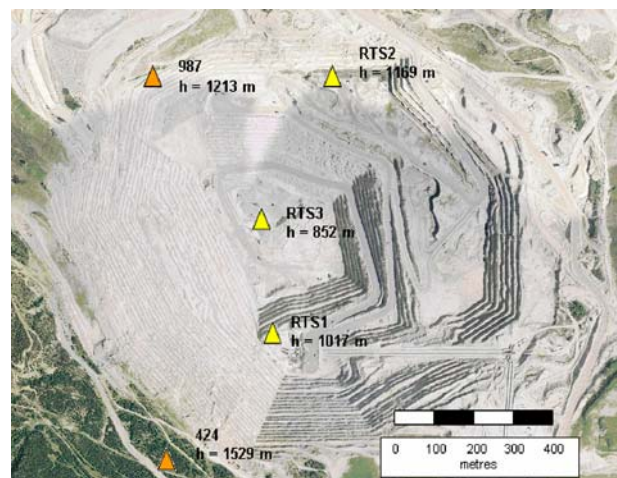


Fig. 5 Large open pit mine test (with station heights shown)

Large open pit mine test

GPS data were collected at five stations in a large open pit mine as illustrated in Fig. 5. Stations 424 and 987 were control stations, while stations RTS1, RTS2 and RTS3 were monitored stations within the pit. Continuous data for 5 days or more were collected. RTS3, located 677 m below

station 424, and having periods of the day during which only three satellites were visible, represented the most challenging deformation monitoring scenario.

Large open pit mine results

The advantages of this filter over batch processing are best revealed by its performance in the environment for which it was designed. Previous analyses of GPS capabilities in this environment were conducted using traditional batch processing methods (Bond 2004). This approach did not allow for an examination of the continuous behavior of the monitored points. Furthermore, cyclic patterns in the up component caused by daily meteorological changes biased the results. There were also periods for which no solution could be achieved. To illustrate the results using batch processing, 1 h, DD, ambiguity-fixed, up-component solutions for baseline 424 to RTS3 are presented in Fig. 6.

To determine if the new processing strategy improved the results, all baselines from stations 424 and 987 were processed using PPMS. Selected baselines are presented here to illustrate the software's capabilities.

Baseline 424 to RTS1 represented the second largest height difference observed. Satellite visibility at RTS1 is not limited as severely as at RTS3. The results of this baseline are illustrated in Fig. 7, from which the following points are noted:

- A change in height of approximately 5 mm occurs shortly after 50 h have elapsed. This was also seen in all other baselines observed from 424 and from 987, except 987 to RTS2 (the shortest baseline located on the same wall of the pit). DD, ambiguity-fixed results before and after this period confirmed this height change. It is thought that geomechanical activity (such as uplift or subsidence) may be responsible.
- The cyclic pattern caused by residual tropospheric biases (illustrated in Fig. 6) has been removed from the up-component. Previous analyses revealed that in order to provide high precision solutions over large height differences, one would have to use 24 h data for the effects of residual tropospheric delay to average out.

Since low elevation satellites are not visible in this environment, estimating a residual tropospheric delay parameter at each station does not significantly improve the results (Bond 2004). This finding indicates that not only does this processing strategy allow for higher precision solutions, but it also allows for more frequent, high precision updates than could normally be achieved using traditional batch processing methods.

- The filter successfully recovered from a data gap at near the 20th hour.

Table 4 compares PPMS results with a 24 h, DD, ambiguity-fixed solution from commercial software after the height change. Standard deviations of the commercial solution are as output by the \pm software.

The initial results of the 424 to RTS3 baseline suffered from the limitations of poor satellite visibility. During periods when only three satellites were visible, the filter solutions would diverge. It is believed that higher order effects of the receiver clock biased the range measurements, since it was no longer able to steer itself. Further work is required to modify the software so that the best known coordinates of the receiver can be used to estimate the receiver clock bias. This value can subsequently be used to correct the range measurements. Quality control had to be added to the software to prevent providing updates during periods in which the range measurements were potentially biased. The results are shown in Fig. 8, from which the following points are noted:

- A change in height occurs after 50 h have elapsed (as seen in Fig. 7)
- The effects of poor satellite visibility have less of an impact on update frequency than with batch processing, since the filter can provide solution updates as soon as sufficient satellites are available. Despite restricting solution updates to periods with greater than three satellites, the longest duration without an update was 74 min. In contrast with the batch processing, there were three periods each day that one would have to wait 2 h for a position update, the precision of which could be poor. After convergence and the height change, a

Fig. 6 424 to RTS3 commercial, up-component solutions

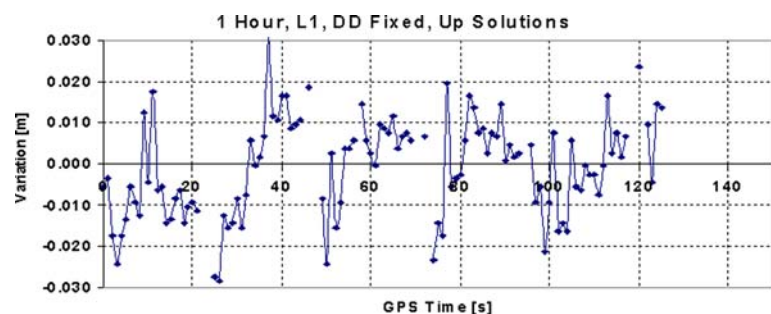


Fig. 7 424 to RTS1 position solutions

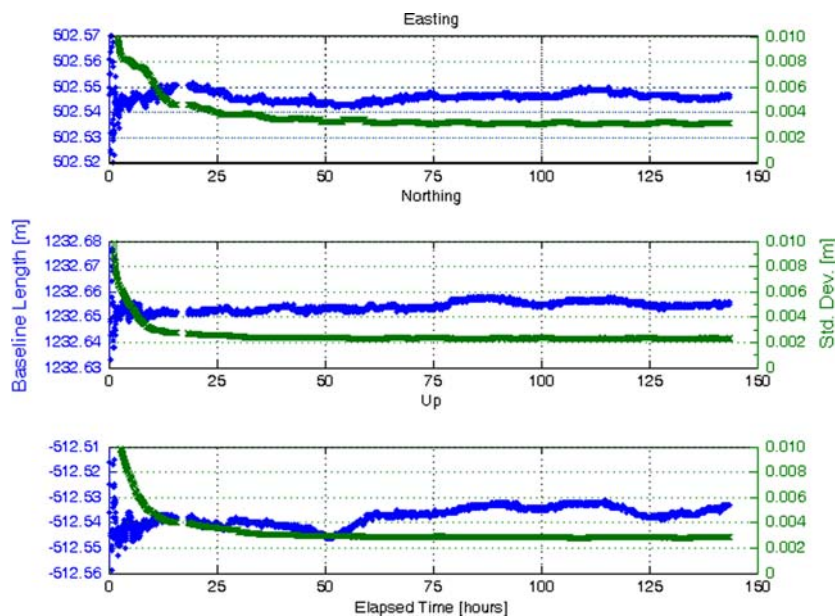


Table 4 424 to RTS1 solution comparison

Solution type	ΔE (m \pm mm)	ΔN (m \pm mm)	ΔU (m \pm mm)
Commercial DD fixed	502.547 \pm 0.5	1232.654 \pm 0.5	-512.528 \pm 0.5
PPMS TD filter	502.545 \pm 3	1232.654 \pm 2	-512.534 \pm 3

peak-to-peak spread of 12 mm in the up-component solutions exists (versus 60 mm in Fig. 6).

Table 5 compares average PPMS results with a 24 h, DD, ambiguity-fixed solution from commercial software. There are centimeter-level discrepancies between the two

solutions, possibly caused by the different approaches to tropospheric modeling. These differences become magnified over large height differences and affect the absolute position values. The error in the height component could be improved by providing solutions only when five or more satellites are available. This comes at the expense of losing position updates for about a third of the day. The use of pseudolites could aid in providing continuous updates with higher precision.

Baseline 987 to RTS2 represents the shortest baseline and a best case scenario in this particular open pit mine. Table 6 compares average PPMS results with a 24 h, DD, ambiguity-fixed solution from commercial software. The filter solutions are shown in Fig. 8.

Fig. 8 424 to RTS3 position solutions

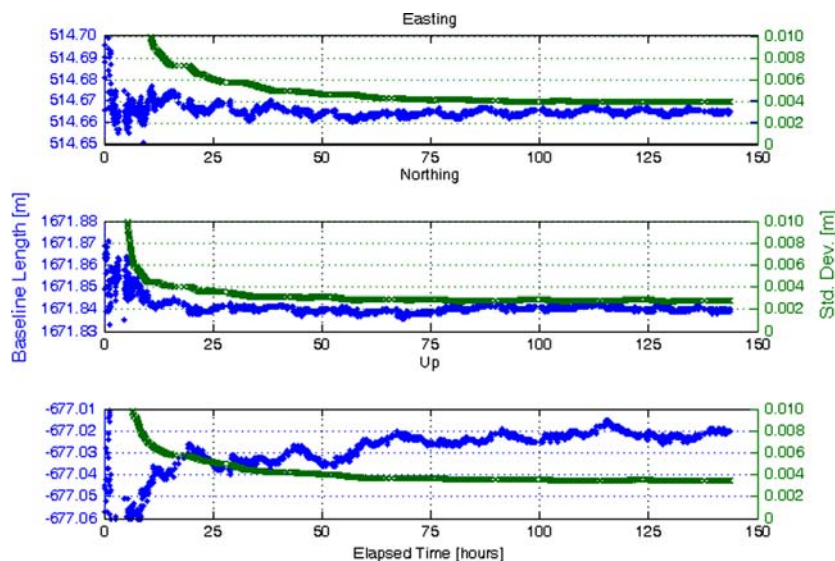


Fig. 9 987 to RTS2 position solutions

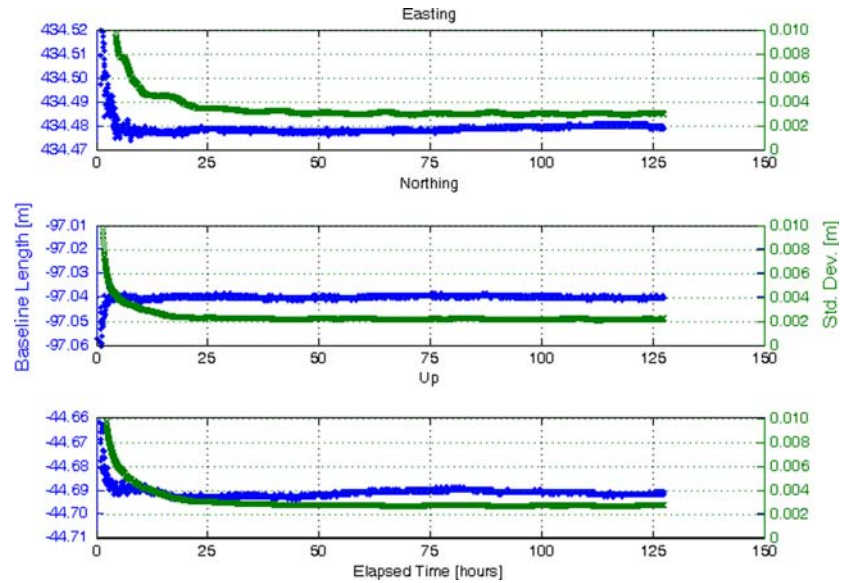


Table 5 424 to RTS3 solution comparison

Solution type	ΔE (m \pm mm)	ΔN (m \pm mm)	ΔU (m \pm mm)
Commercial DD fixed	514.685 \pm 0.7	1671.852 \pm 0.8	-677.044 \pm 2
PPMS TD filter	514.675 \pm 4	1671.841 \pm 3	-677.025 \pm 4

Table 6 987 to RTS2 solution comparison

Solution type	ΔE (m \pm mm)	ΔN (m \pm mm)	ΔU (m \pm mm)
Commercial DD fixed	434.480 \pm 0.4	-97.040 \pm 0.4	-44.694 \pm 0.9
PPMS TD filter	434.479 \pm 3	-97.040 \pm 2	-44.692 \pm 3

Conclusions

In response to the need for continuous GPS position updates in harsh deformation monitoring environments, a software is being developed that employs TD carrier-phase measurements in a delayed-state Kalman filter. Besides the obvious benefit of not having to deal with the nuances of cycle slip repair, it was shown that the TD observation can be used to significantly reduce the effects of residual tropospheric delay biases. The cost of using the TD observable is a slower convergence time than with the DD observable. This is generally not a concern for long-term deformation monitoring projects.

Depending upon client requirements and environmental conditions, the filter can be adjusted to be more or less sensitive to the observations. Quicker detection time currently comes at the expense of more noise in the solutions. A slow, 25 mm displacement was detected within 30 min of the full displacement with sigma values in E , N and U of ± 10 mm or better. The same displacement could also be detected in less than 5 h with sigma values in E , N and U of ± 5 mm or better. The software works best for detecting

long period deformations (e.g., 20 mm per day or less) for which sigma values of 1–2 mm are attained in all three solution components. The filter would benefit from allowing the process noise to be adaptive.

The extreme conditions of harsh environments limit the frequency at which high precision updates could be provided. Using PPMS, updates could be provided at least every 75 min, as opposed to every 24 h using traditional processing methods. More frequent updates could be provided by utilizing pseudolite technology. PPMS is currently being enhanced to offer this capability.

Acknowledgments This research was funded by the Natural Sciences and Engineering Research Council of Canada (NSERC) and by the Canadian Wireless Telecommunications Association (CTWA). Special thanks are given to Tomas Beran of Focus Surveys Ltd for his comments and suggestions.

References

- Beutler G, Bauersima I, Gurtner W, Rothacher M, Schildknecht T, Gieger A (1988) Atmospheric refraction and other important biases in GPS carrier phase observations. Atmospheric effects on

- geodetic space measurements. Monograph 12, School of Surveying, University of New South Wales, pp 15–43
- Bond J (2004) An investigation on the use of GPS for deformation monitoring in open pit mines. M.Sc.E. thesis, Technical Report No. 222, Department of Geodesy and Geomatics Engineering, University of New Brunswick, Fredericton, pp 1–140
- Bond J, Chrzanowski A, Wilkins F (2005) Using GPS for augmenting deformation monitoring systems in open pit mines—problems and solutions. *Geomatica* 59(1):73–82
- Brown RG, Hwang PYC (1997) Introduction to random signals and applied kalman filtering, 3rd edn. Wiley, New York, pp 1–484
- Chrzanowski A, Wilkins F (2006) Accuracy evaluation of geodetic monitoring of deformations in large open pit mines. Proceedings of the 12th FIG symposium on deformation measurements, Baden, Austria, 21–24 May, CD ROM
- Collins JP, Langley RB (1999) Nominal and extreme error performance of the UNB3 tropospheric delay model. Department of Geodesy and Geomatics Engineering Technical Report No. 204, University of New Brunswick, Fredericton, pp 1–173
- Kim D, Langley RB (2002) Instantaneous real-time cycle-slip correction for quality control of GPS carrier-phase measurements. *J Inst Navigation* 49(4):205–232
- Kim D, Langley RB, Bond J, Chrzanowski A (2003) Local deformation monitoring using GPS in an open pit mine: initial study. *GPS Solut* 7(3):176–185. doi:10.1007/s10291-003-0075-1
- Leick A (1994) *GPS Satellite Surveying*. 2nd edn. Wiley, New York, pp 1–560
- Remondi BW (1984) Using the global positioning system (GPS) phase observable for relative geodesy: modeling, processing, and results. Doctoral thesis, Center for Space Research, University of Texas at Austin, pp 1–324.
- Remondi BW, Brown G (2000) Triple differencing with Kalman filtering: making it work. *GPS Solut* 3(3):58–64
- Rizos C (1999) Principles and practice of GPS surveying, Section 9.1.5: outlier testing and residuals. http://www.gmat.unsw.edu.au/snap/gps/gps_survey/principles_gps.htm
- Teunissen PJG (1998) *GPS for geodesy*. Chap 7: quality control and GPS, 2nd edn. Springer, Heidelberg, pp 271–318
- Wilkins R, Bastin G, Chrzanowski A (2003) Monitoring of structures and steep embankments: a fully automated approach. Paper presented at CSCE Annual Conference, Moncton, NB, Canada, June 4–7, 2003. Available at: <http://www.ccge.unb.ca>